한국정밀공학회지 제 16 권 제 1 호 (1999 년 1 월)
Journal of the Korean Society of Precision Engineering, Vol. 16, No. 1, January 1999.

순간 발산지수의 카오스계에의 응용, 파트 2: 실험 및 힘-위상 (Force-State Mapping) 방법과의 비교

신기홍*

Application of the Instantaneous Lyapunov Exponent and Chaotic Systems, Part 2: Experiment and Comparison with the Force-State Mapping Method

Kihong Shin*

ABSTRACT

본 논문은 '파트 1' 에 그 기초를 두었으며, 실제 실험 상황에의 응용예를 들었다. 보편적인 '이중-우물 위치 진동기(double-well potential vibrator)'를 외부 공기압 감쇠기를 장치할 수 있도록 수정하였다. 감쇠는 높음 또는 낮음 으로 조정할 수 있도록 하였다. 이 실험계는 주기운동부터 카오스 운동까지 다양한 동적 특성을 보여준다. 힘-위상(Force-State Mapping) 방법이 선형상태 및 카오스상태에 응용되었으며, 특히 감쇠의 높고 낮음의 파악에 그 중점을 두었다. 그리고, 부분발산지수들(Short term averaged Lyapunov exponents)의 합이 또한 감쇠를 파악함과 동시에 높은 감쇠에서 낮은 감쇠로의 변화를 감시할 수 있음을 보였다. 이 두가지 방법들을 비교하였으며 논하였다.

Key Words : Lyapunov Exponent(발산지수), Instantaneous Lyapunov Exponents(순간발산지수), Force-State Mapping(힘-위상도), Chaos(카오스), Phase Space(위상공간)

1. Introduction

Chaotic motion of the double-well potential vibrator have been extensively studied over the last couple of decades. For example, Moon and Holmes [1] studied motions of a thin steel beam buckled between two magnets, and established firm theoretical and experimental evidence of chaotic behaviour of this type of vibrator. However, not many articles can be found relating to system identification or identifying some physical parameters of the system. This paper is mainly focused on identifying system parameters, and also on tracking changes of a parameter (characterising damping).

In general, system identification methods for dynamical systems may be classified into two groups: one is the parametric approach and the other non-parametric. Parametric methods seek to determine the values of parameters in an assumed model of the system to be identified, while non-parametric methods produce the best functional representation of the system without a priori assumptions about the system model. For system identification of non-linear systems, if all state variables, the acceleration signal and input signal are available

* ISVR, University of Southampton, Southampton SO17 1BJ UK

together with knowledge of the mass, we can use the force-state mapping method. The 'force-state mapping' technique, which is a non-parametric method, was first introduced by Masri and Caughey in 1979 [2]. Later in 1985, O'Donell and Crawley independently developed a similar method and named it the 'force-state mapping' [3 - 7]. Since then, this technique has been applied to various engineering fields and developed further, especially by Worden and Tomlinson [8 -10], Al-Hadid and Wright [11 - 15], and Lo [16]. The usefulness of this method is that one can estimate (all) the system parameters. This method has been applied to various non-linear systems over the last couple of decades, but it has not been reported for chaotic systems. This paper also demonstrates how well the force-state mapping technique can be applied to a practical chaotic system.

The beam studied in this paper is similar to the "Moon Beam" in reference [1] in principle, and its dynamics are very similar to the Duffing type oscillator. However, unlike the "Moon Beam", the shaker is used directly on the cantilever beam and a dash-pot air damper is also introduced to control the amount of damping in the system. The damper is set to produce two cases by adjusting the damper plug giving high and low damping. When the magnets are removed the beam becomes a simple linear cantilever beam. The force-state mapping method is applied to this experimental set-up to identify system parameters for both the linear system (without magnets) and the non-linear system (with magnets). The excitation signal in the case of the linear system is an amplitude modulated sinusoidal signal. For a non-linear system, the amplitude modulated sinusoidal signal may not be successful since the motion of the beam behaves in a complex way and does not cover the state space effectively when the input amplitude gets large. This is due to the magnets which attract the beam. However, when the beam is excited by a single sinusoidal signal with a certain amplitude level, its motion becomes chaotic. Although the input signal is a single sinusoid, because the motion is chaotic it covers a wide range of the state space. Thus it makes it possible to use the force-state mapping method. In this case, however, one must be very careful about the estimation of the "effective mass" which will be discussed later.

One of the objectives of this paper is to create a system whose 'condition' (in this case damping) may change quite quickly during running conditions and to detect this change. The damping is changed from being high to low. If the system is linear it may be easily monitored by many other conventional methods. However, if the system is operating in a chaotic region many conventional methods may not applicable. As described in Part 1, it may be possible to detect this change of damping by using the sum of SLEs (Short-term averaged Lyapunov Exponents). The values of the sum of SLEs are monitored through high damping to low damping, and are compared with the values obtained from the force-state mapping method. In theory, if the damping term is linear then the sum of SLEs should be equal to the negative of the normalised damping parameter (normalised with respect to the mass). It will be shown that experimental results show good agreement between the force-state mapping technique and the sum of SLEs.

2. Description of the Experiments and Equations of Motion

The mechanical system studied here is a cantilever beam buckled by two magnets as illustrated in Fig. 1. This system is similar to the magneto-elastic oscillator of Moon and Holmes [1]. They used a very flexible thin steel beam clamped at one end, and the whole device was driven by a shaker. However, their beam was very thin (0.23mm), so it was difficult to introduce an external damper. Thus, for the experiment in this paper, a device was constructed which can accommodate a dash-pot damper. A thin steel beam with dimensions 365mm×25mm×1mm is clamped at the top of the experimental rig. At 70mm from the free end of the beam, a dash-pot air damper is introduced. This damper can be controlled by adjusting the amount of air flow using a plug provided in the damper. Two magnets are secured on a steel plate near the free end of the beam to provide non-linear buckling forces. A sinusoidal signal from a signal generator is fed to an electromagnetic shaker through a power amplifier, with a signal be generated by a PC. The beam is then excited by an

electromagnetic shaker at 60mm from the clamped end of the beam. A force transducer is placed between the beam and the shaker, and a full bridge strain gauge is attached near the clamped end of the beam. The force and strain gauge signals are fed to an oscilloscope and a PC with a data acquisition system. Provided that the motion of the beam is dominated by one mode only, the strain gauge signal can be transformed to a corresponding displacement signal, since the bending strain (ε_x) is proportional to the lateral displacement (y) such that

$$\varepsilon_x = ky. \tag{1}$$

The constant k is found by measuring the strain gauge bridge output for a given static displacement. For this experimental set-up, we can directly relate the beam tip displacement and the output of the signal conditioner (amplifier) of the bridge.

This experimental set-up may be depicted as shown in Fig. 2 and 3. Applying Euler beam equations and considering magnetic forces, of which details can be found in [1], the equation of motion can be written as

$$EI\frac{\partial^4 v(x,t)}{\partial x^4} + m\frac{\partial^2 v(x,t)}{\partial t^2} + c_1\delta(x-l_2)\frac{\partial v(x,t)}{\partial t} + \frac{\partial}{\partial x}\left[\kappa\frac{\partial v(x,t)}{\partial x}\right] - \frac{\partial}{\partial x}\left[T\frac{\partial v(x,t)}{\partial x}\right] = F_y + f(x,t) \tag{2}$$

where E is Young's modulus, I is the second moment of area, m=ρA is the mass per unit length of the beam, and f(x,t) is the applied force per unit length along the beam. The boundary conditions are

$$v(0,t)=0,\quad \left.\frac{\partial v(x,t)}{\partial x}\right|_{x=0}=0 \quad \text{at } x=0$$

$$\left.\frac{\partial^2 v(x,t)}{\partial x^2}\right|_{x=L}=0,\quad T=0,$$

$$EI\left.\frac{\partial^3 v(x,t)}{\partial x^3}\right|_{x=L} + \kappa\left.\frac{\partial v(x,t)}{\partial x}\right|_{x=L}=0 \quad \text{at } x=L$$

$\frac{\partial}{\partial x}\left[\kappa\frac{\partial v(x,t)}{\partial x}\right]$ is called the body couple gradient [1] for moment equilibrium about the z-axis normal to the x-y plane, and $\kappa>0$ is related to the external magnetic field, and depends on the amplitude of the beam. $\frac{\partial}{\partial x}\left[T\frac{\partial v(x,t)}{\partial x}\right]$ represents the restoring force on the beam due to the tension T which is created by the axial magnetic force, i.e., $T(x) = T(L) - \int_0^x F_x dx$. F_x, and F_y are defined as the magnetic forces per unit length along the beam with respect to the x-axis and y-axis respectively, and these forces depend on the amplitude of the beam. To solve equation (2), Galerkin's method is used. A suitable set of orthogonal basis functions $\phi_n(x)$, which satisfy the boundary conditions, is chosen and the unknown displacement $v(x,t)$ is given by

$$v(x,t) = \sum_{n=1}^{\infty} q_n(t)\phi_n(x) \tag{3}$$

Substituting (3) into the equation of motion and taking the inner product (i.e., integrating over the beam length) with $\phi_k(x)$, k=1, 2, ..., results in an infinite set of second order ordinary differential equations. However, if we assume the forcing frequency is near the first mode, and the first mode is dominant in the motion of the beam, the single degree of freedom approximation can be made as

$$v(x,t) = q(t)\phi(x) \tag{4}$$

where, $\phi(x)$ satisfies the boundary conditions

$$\phi(0)=0,\quad \left.\frac{d\phi(x)}{dx}\right|_{x=0}=0 \quad \text{at } x=0$$

$$\left.\frac{d^2\phi(x)}{dx^2}\right|_{x=L}=0,\quad EI\left.\frac{d^3\phi(x)}{dx^3}\right|_{x=L} + \kappa\left.\frac{d\phi(x)}{dx}\right|_{x=L}=0 \quad \text{at } x=L$$

and the mode shape can be normalised, i.e., $\int_0^L \phi^2(x)dx = 1$.

By single mode Galerkin's approximation, the resulting differential equation becomes

$$m\ddot{q}(t) + \left\{c_1\phi(l_2)^2\right\}\dot{q}(t) + \left\{EI\int_0^L\left[\frac{d^2\phi}{dx^2}\right]dx + \int_0^L(T-\kappa)\left[\frac{d^2\phi}{dx^2}\right]dx\right\}q(t) = \int_0^L F_y\phi dx + \int_0^L f(x,t)\phi dx \tag{5}$$

If we assume that the magnetic field acts primarily at the beam tip, i.e.,

$F_y = F_y\delta(x-L)$, $F_x = F_x\delta(x-L)$, $\kappa = K\delta(x-L)$, $T = F_x$

and if the harmonic external forcing term is located at one point as shown in Fig. 2, i.e.,

$$f(x,t) = A_0\cos(\omega t)\delta(x-l_1)$$

then equation (5) becomes

$$m\ddot{q}(t) + \left\{c_1\phi(l_2)^2\right\}\dot{q}(t) + k_1 q(t) - F_y(q)\varphi(L) = A_0\cos(\omega t)\phi(l_1) \tag{6}$$

where

$$k_1 = \left\{ EI\int_0^L \left[\frac{d^2\phi}{dx^2}\right]dx - K\left[\frac{d\phi(x)}{dx}\Big|_{x=L}\right]^2 + F_x(q)\int_0^L \left[\frac{d\phi(x)}{dx}\Big|_{x=L}\right]^2 dx \right\} \quad (7)$$

To complete the model, we follow the assumptions made concluding the functions $F_x(q)$, $F_y(q)$ in reference [1]

$$F_x(q) = F_x = const.,$$

$$F_y(q) = \frac{1}{\phi(L)}\left(\alpha_1 q(t) + \beta q^3(t) + \text{higher order terms}\right) \quad (8)$$

Thus equation (6) becomes

$$m\ddot{q}(t) + c\dot{q}(t) - \alpha q(t) + \beta q^3(t) = A\cos(\omega t) \quad (9)$$

where, $c = c_1\phi(l_2)$, $\alpha = \alpha_1 - k_1$, $A = A_0\phi(l_1)$.

Thus equation (9) is in the form of a Duffing equation, and so the experimental set-up (Fig. 1) can be considered as a Duffing oscillator provided that the motion of the beam is dominated by the lowest mode only.

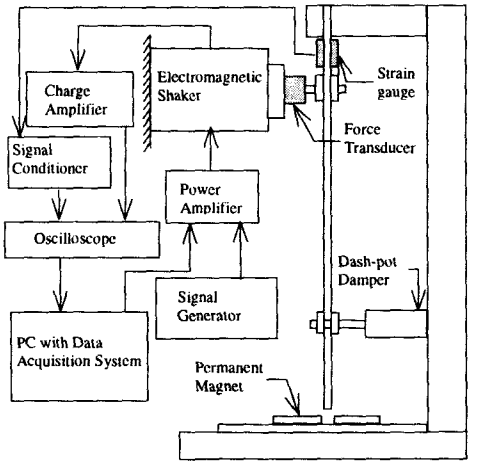

Fig. 1 Experimental Set-up

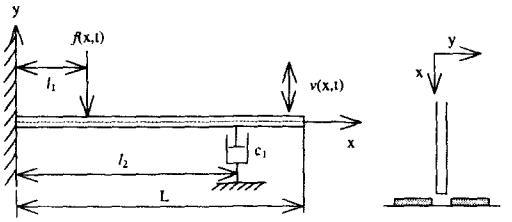

Fig. 2 Experimental Set-up

Fig. 3 Experimental Set-up

The Duffing oscillator is a single degree of freedom non-linear system with two stable equilibrium points and an unstable equilibrium point. Chaotic motion from a Duffing oscillator is generated when the motion evolves around the two stable equilibrium points almost irregularly. In the experimental set-up, two stable equilibrium points are the centre of each magnet, and the unstable equilibrium point is between the two magnets. To make sure that the beam behaves like a single degree of freedom system, the motion of the beam should be dominated by its lowest mode during the experiment. Assuming that the excitation frequency is near the first natural frequency of the linear system (without magnets) results in the motion of the beam being dominated by the lowest mode, we choose a sinusoidal signal with a single frequency near the first natural frequency of the beam. The natural frequencies of the beam without magnets (i.e., in linear state) were measured, and the lowest natural frequency is about 7.1 Hz. The introduction of the magnets is to increase stiffness and introduce non-linearity, but for low amplitude motion the 'natural frequency' is shifted upwards slightly. During the experiment, the beam is excited just below the first natural frequency (7Hz) without the magnets, and it is observed that this results in the motion of the beam being dominated by the first mode.

It is now briefly demonstrated how the experimental system changes from periodic motion to chaotic motion by presenting both time series and pseudo phase space (reconstructed phase portrait using the 'method of delays') for each case of different motions. Starting with a small amplitude for the input signal, the motions of the beam are examined by gradually increasing the amplitude of the input signal with a fixed frequency (7Hz). When the amplitude of the input signal is small, the beam oscillates around one of the equilibrium points. The fundamental period of the motion is the same as the period of the input signal, i.e., period-1 motion as shown in Fig. 4(a) and (b). As the amplitude increases the motion becomes period-2, period-3, etc., and finally it becomes chaotic. These are shown in Fig. 4. It is also found experimentally that the motion after period-3 is very sensitive to amplitude applied, so a small increase of amplitude causes chaotic motion. Thus, it is very difficult to observe the higher order subharmonic motions beyond period-3. This may be due to the finite precision of the experimental devices which cannot control the input amplitude precisely. However, from Fig. 4, we can see that chaotic motion arises after

subharmonic motion.

It has been shown how the experimental set-up behaves like the Duffing equation in a specific case, and several types of motion of the beam, depending on the amplitude of excitations, have been presented. In the following sections, system parameters in (9) are obtained from the force-state mapping technique, and a comparison is made of the damping parameter obtained by the force-state mapping method and the short-term averaged Lyapunov exponents.

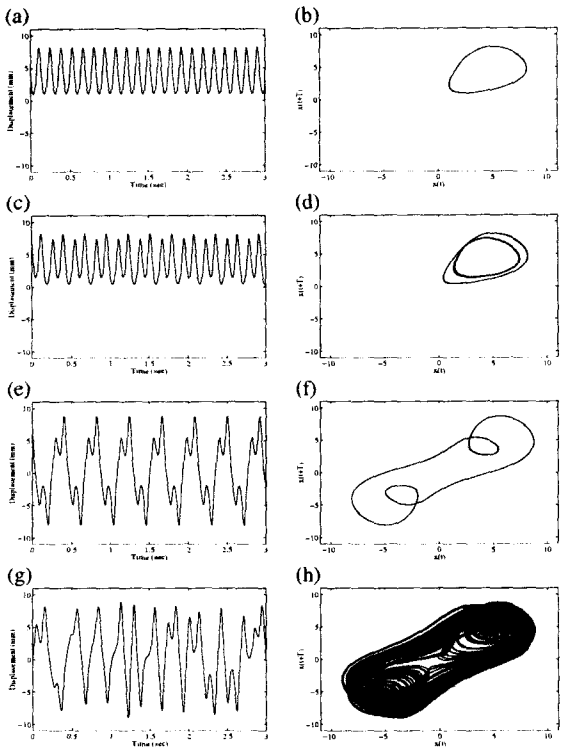

Fig. 4 Different types of motions of the beam (forcing frequency 7Hz) Pseudo phase portraits are constructed by the method of delays with delay time T=0.026 sec. x(t) denotes the displacement
(a) Time series of the period-1 motion
(b) Pseudo phase portrait of period-1 motion
(c) Time series of the period-2 motion
(d) Pseudo phase portrait of period-2 motion
(e) Time series of the period-3 motion
(f) Pseudo phase portrait of period-3 motion
(g) Time series of the chaotic motion
(h) Pseudo phase portrait of chaotic motion

3. System Identification using the Force-State Mapping Method

We consider the equation of motion of the SDOF system

$$m\ddot{x} + f(x,\dot{x}) = F(t) \tag{10}$$

where $f(x,\dot{x})$ is a function which denotes the restoring force of the system. Rearranging (10) we have

$$f(x,\dot{x}) = F(t) - m\ddot{x} = F_{net} \tag{11}$$

If we know the applied force, mass, and acceleration signal, then we can construct a 3-dimensional plot of 'F_{net}' versus 'x' and '$\dot{x}$'. The state variables (x and $\dot{x}$) can be usually found by direct measurements or through integration of $\ddot{x}$. If the net force (F_{net}) is only a function of the state variables, then the 3-dimensional plot produces a unique surface and the surface will be independent of the time history of the applied force. Therefore, any type of applied force can be used. However, the ability to produce a complete 'force-state map' requires that the force input signal excites displacement (x) and velocity ($\dot{x}$) which adequately 'cover' the state space in such a way that the measurements are reasonably dense within the space. If there is a region in the state space which is not excited by the applied force, then there will be a 'hole' in the surface of the force-state map. Thus, the commonly used input force signals are random signals and modulated sinusoidal signals. Once we have obtained the necessary signals (F_{net}, x and $\dot{x}$), then the state signals are divided into 'grids' with designated 'representative points'. A representative point can be obtained by averaging all the 'F_{net}' values whose corresponding state (x and $\dot{x}$) fall into the pre-determined specific grid [16]. This results in 'x' being a row×1 vector, '$\dot{x}$' being a col×1 vector, and 'F_{net}' being a row×col matrix, where 'row' and 'col' are the number of grids for each signal. When this process is done, the state parameters can be obtained by curve fitting to the surface (e.g. Chebyshev polynomials by Masri *et al.* [2]). In this paper, ordinary polynomials are used for the curve fitting, and the force-state mapping method is applied to both experimental linear systems and chaotic systems. In order to successfully apply the

force-state mapping method, there are many things to be carefully considered. Any phase mismatches of devices will degrade the quality of the surface and should be avoided. For example, the charge amplifier used in this experiment had a 180 degree phase shift which had to be accounted, and different devices have different phase delays associated with them. These characteristics must be carefully considered and accounted for. In general, it may be difficult to measure all the necessary signals simultaneously, so one usually measures acceleration and then obtains displacement and velocity signals by either time domain integration or frequency domain integration. However during chaotic motion in this experiment, which results in swinging from one equilibrium point to another, this produces large negative and positive offsets in measurements, making it difficult to use integration methods, since offset introduces a drifting effect. Thus, we use numerical differentiation after measuring the displacement signal which is obtained via the strain gauge bridge output. If x(n) is the measured discrete displacement time series with sampling rate 1/T, then the velocity signal is obtained by using central difference approximation [17], i.e.,

$$x'(n) = \frac{x(n-2) - 8x(n-1) + 8x(n+1) - x(n+2)}{12T} \quad (12)$$

One drawback of numerical differentiation is noise on the measured signal. An 'insignificant' noise in the displacement signal may cause a very noisy acceleration for high frequency components. This problem can be alleviated by using the 'Iterative SVD method' which was developed by Shin [18]. It was shown that if the sampling rate is very high compared to the forcing frequency, then one can almost blindly use this method. Examples of noise reduction are shown together with the experimental results for linear systems. A particular problem is the estimation of mass, which is also discussed.

3.1 Linear systems

If we do not introduce the two permanent magnets and excitation is not too large, the experimental set-up becomes a simple linear cantilever beam. So the equation of motion for one mode (9) can be simply written as

$$c\dot{q}(t) + kq(t) = F(t) - m_e\ddot{q}(t) = F_{net} \quad (13)$$

We now estimate the system parameters 'c and k' by using the force-state mapping method. The input forcing signal is generated in the PC and then, through the DAC (Digital-Analogue Converter) and amplifier, it is fed to the shaker. The input signal used here is an amplitude modulated signal as shown in Fig. 5.

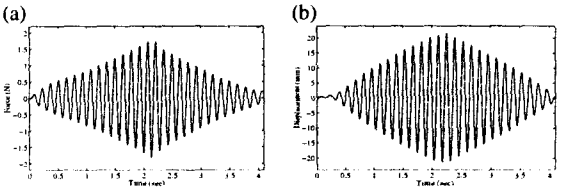

Fig. 5 Input, output signal used for a linear system identification (forcing frequency 7Hz)
(a) Actual input force signal measured from a force transducer
(b) Measured displacement signal converted from the strain gauge bridge output

Even in a simple linear system, correct estimation of the effective mass 'm_e' is critical and has been studied extensively by a number of authors. If the geometry is simple like a cantilever beam, the effective mass (modal mass of the first mode) can be obtained directly by

$$m_e = \int_0^L m\phi^2 dx = \left(\frac{m}{\beta_1}\right)\int_0^{\beta_1 L}\phi^2 d\beta_1 x = \frac{3.48m}{\beta_1} \quad (14)$$

where, m is mass per unit length of the beam, and $\beta_1 L$ = 1.8751. The mass estimated by (14) for the experimental set-up is m_e=0.13kg. However, for this estimated mass, the effects of additional masses are not included, i.e., dynamic mass of the shaker and the mass of the force transducer introduce additional mass. Because the cantilever beam is very light, we must consider the additional masses. Thus, we use the sensitivity approach method developed by Al-Hadid *et al.* [12 - 14]. Reference [14] briefly summarises the basic idea of this approach. Given a single degree of freedom system of the form of equation (10), if we use an incorrect mass '$\hat{m}$' (assumed mass) then we estimate the incorrect restoring force '$f(x,\dot{x})$'.

If the system is linear, then $\hat{f}(x,\dot{x}) = \hat{c}\dot{x} + \hat{k}x$, where $\hat{c}$ is the estimated damping and $\hat{k}$ is the estimated stiffness. For a linear system and a single

sinusoidal frequency excitation (ω), the relationship between the estimated mass and the estimated stiffness is given by [14]

$$\hat{k} = (k - \omega^2 m) + \omega^2 \hat{m} \qquad (15)$$

where, 'm' and 'k' are exact mass and stiffness respectively. Thus it is shown that the relationship between $\hat{m}$ and $\hat{k}$ is linear. Thus we can find the intersection point by plotting lines (estimated stiffness versus assumed mass) found from curve fits to measurements taken at two or more different excitation frequencies, assuming two initial mass values. In general, the system parameter for the plot is the stiffness term, but any system parameters can be used. If the system is a single degree of freedom system, any lines must intersect at one point. This relationship is also true for non-linear systems but depends on excitation amplitude [14]. However for a continuous system like the thin cantilever beam used in this experiment, although the excitation frequencies are very near the first resonance frequency, the lines do not intersect at one point but vary from frequency to frequency as shown in Fig. 6(a). This may be caused by the interference of higher modes. If this is true, the effective mass is different at each driving frequency although the overall behaviour of the system is like a single degree of freedom system. However, the effective masses at neighbouring frequencies should not differ greatly from each other. Thus, in this experiment, we first decide the driving frequency and then perform the sensitivity approach using frequencies very near the driving frequency. We choose the driving frequency at 7Hz which is very close to the first natural frequency of the beam, and use the frequencies at 6.8Hz and 7.2Hz for the sensitivity approach. This is shown in Fig. 6(b), and the estimated effective mass is 0.52kg. This method is carried out in exactly the same way for the non-linear systems described in section 3.2.

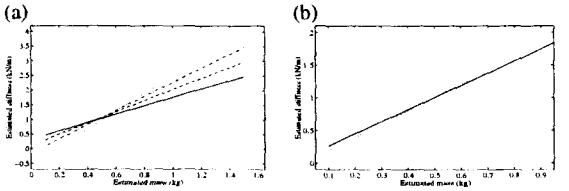

Fig. 6 Mass estimation plot for a linear system using the sensitivity approach

(a) Estimated mass is varying from 0.42kg to 0.65kg (Forcing frequencies: 6Hz, 7Hz, 8Hz and 9Hz from solid line to dotted line)
(b) Estimated mass is 0.52kg (Forcing frequency: 6.8Hz for solid line and 7.2Hz for dotted line)

Once the correct effective mass is estimated, one can now produce the surface representation of the system. However, noise introduced through the numerical differentiation cannot be ignored. A 3-dimensional plot of net force versus state variables without any noise reduction technique is shown in Fig. 7(a). Using the 'Iterative SVD method', this noise can be significantly reduced as shown in Fig. 7(b). The details of this noise reduction technique can be found in [18].

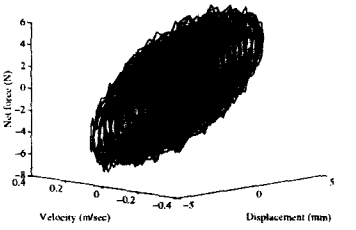

Fig. 7(a) Force-state plot of a linear system without the noise reduction technique (high damping)

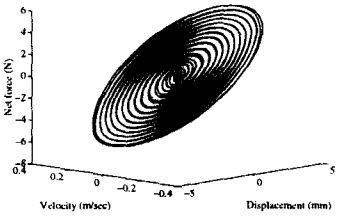

Fig. 7(b) Force-state plot of a linear system with the noise reduction technique (high damping)

The 3-dimensional surface representation is shown in Fig. 8(a) for the highly damped system, and in Fig. 8(b) for the case of the weakly damped system. From Fig. 8, the estimated values of the parameters by polynomial curve fitting are 'c = 7.3 N·s/m and k = 1.008 kN/m' for the case of high damping, and are 'c = 2.7 N·s/m and k = 1.007 kN/m' for the case of low damping. The results are promising since the change of the property of air dash-pot damper (which is assumed to be linear) causes only a

change of the damping coefficient while the stiffness term remains almost the same.

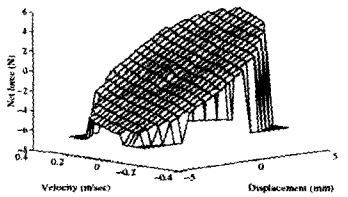

Fig. 8(a) Surface representation of the force-state map of a linear system (high damping)
Estimated values of parameters: c = 7.3 N·s/m and k = 1.008 kN/m

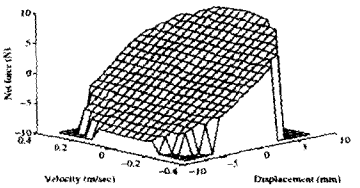

Fig. 8(b) Surface representation of the force-state map of a linear system (low damping)
Estimated values of parameters: c = 2.7 N·s/m and k = 1.007 kN/m

3.2 Non-linear (chaotic) system

Equation of motion (9) can be rearranged as

$$c\dot{q}(t) - \alpha q(t) + \beta q^3(t) = F(t) - m_e\ddot{q}(t) = F_{net} \quad (16)$$

For the forcing signal 'F(t)', one may attempt to use the same signal as in the case of the linear system. However, it was found that the short duration of the amplitude modulated signal fails to excite a large area of the state space. The motion of the beam becomes chaotic as soon as the amplitude gets large, producing a 'hole' in the state space. However, if we excite the beam with a single sinusoidal signal in a chaotic regime over a long time, the motion is chaotic and a large area of state space will be covered. Thus the forcing signal for this case is chosen as a sinusoidal signal creating a chaotic regime.

The effective mass estimation is carried out in the same way as described in section 3.1. As shown in Fig. 9, the effective mass is estimated as 0.77kg. For linear systems, any assumed masses can be used to estimate the effective mass of the system.

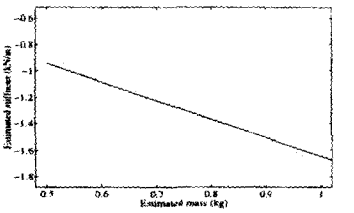

Fig. 9 Mass estimation plot for a chaotic system using the sensitivity approach
Estimated mass is 0.77kg
(Forcing frequency: 6.8Hz for solid line and 7.2Hz for dotted line)

However, one must be careful when the sensitivity approach is used for a chaotic system. Unlike the linear system, the 3-dimensional plot of net force versus state space using a significantly different mass from the true effective mass will result in almost no structure. This makes it impossible to estimate the effective mass, since the estimated system parameters corresponding to the assumed mass is obtained from the estimated force-state surface constructed by using the assumed mass. An example of a bad choice of assumed mass is shown in Fig. 10(a) with an assumed mass 0.2kg, and Fig. 10(b) shows the example of right choice of the assumed mass (0.7 kg).

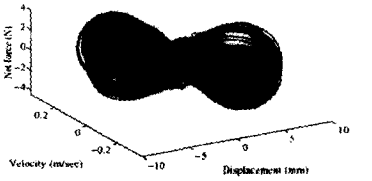

Fig. 10(a) Bad choice of the assumed mass
Force-state plot of a chaotic system with an assumed mass 0.2kg (low damping)

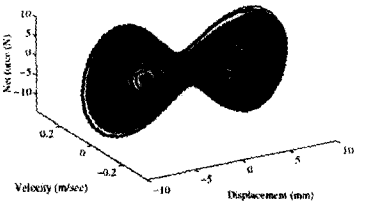

Fig. 10(b) Right choice of the assumed mass
Force-state plot of a chaotic system with an assumed mass 0.7kg (low damping)

Thus assumed mass must be chosen carefully. We simply use the sensitivity approach on a trial and error basis, i.e., one can construct the 3-dimensional plot using from a very small assumed mass to a very large assumed mass by incrementing the assumed mass, and finding the region where the structure is revealed. Using the estimated effective mass, we produce the surface representation of the system. The surface representation is shown in Fig. 11(a) for the high damping system, and in Fig. 11(b) for the case of low damping.

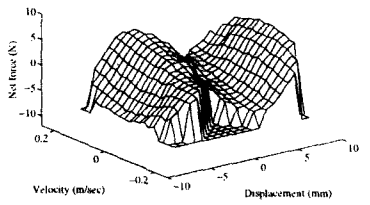

Fig. 11(a) Surface representation of the force-state map of a chaotic system (high damping)
Estimated values of parameters:
$c = 8.6$ N·s/m, $\alpha = -1.3$ kN/m, and $\beta = 56.1$ MN/m^3

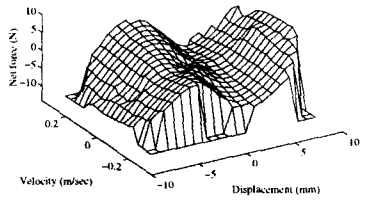

Fig. 11(b) Surface representation of the force-state map of a chaotic system (low damping)
Estimated values of parameters:
$c = 3.0$ N·s/m, $\alpha = -1.4$ kN/m, and $\beta = 54.9$ MN/m^3

From these Fig., the estimated values of the parameters by polynomial curve fitting are 'c = 8.6 N·s/m, α = 1.3 kN/m, and β = 56.1 MN/m^3' for the case of high damping, and are 'c = 3.0 N·s/m, α = 1.4 kN/m, and β = 54.9 MN/m^3' for the case of low damping. The results are almost the same as the case of linear systems, i.e., only an increase of damping coefficient while the other parameters remain almost the same, but the damping coefficient of the chaotic system should not differ from that of the corresponding linear system. However, there is a small difference between the linear system and chaotic system in the estimation of the damping parameter. In spite of this small difference, considering many aspects of measurements and numerical procedures, we can consider the difference is insignificant, and the results can be considered as satisfactory.

4. Detection of Changes in Damping of the System using the Sum of Short-term Averaged Lyapunov Exponents

This section demonstrates the use of the sum of ILEs (Instantaneous Lyapunov Exponents) for experimental data. From a measured time series (displacement signal for this experiment), we estimate the ILEs, and then produce the SLEs (Short-term averaged Lyapunov Exponents) to find whether there is a significant change of damping. As mentioned in Part 1, the sum of Lyapunov exponents describes the global damping property which is related to the rate of volume contraction in phase space. However, the sum of SLEs gives the local damping property of the system, thus enabling us to track the changes of damping. In this section, we use the same techniques and processes described in the Part I. We first measure a time series, and reconstruct the phase portrait by using the method of delays or by the SVD. From the reconstructed phase portrait, we can now estimate the SLEs.

We here consider the same two chaotic systems as in the previous section, i.e., one has high damping and the other has low damping, with all configurations of the experiment remaining the same. In this section, we use the measured displacement signal for following analysis. The reconstructed phase portraits by the SVD of both systems (high damping and low damping) are shown in Fig. 12(a) and (b). Once the phase portraits are reconstructed, ILEs can be estimated as well as the SLEs. The sum of SLEs is shown in Fig. 12(c) and (d) for the case of high damping and low damping respectively, and the average values of the sum of SLEs are −10.1 and −4.5 respectively. These average values are taken from several segments of the sum of SLEs, and the SLEs are calculated by averaging about 60 previous forcing periods of ILEs. From the sum of SLEs, we can also

estimate the damping parameters by using the effective mass (0.77kg) estimated in the previous section. The estimated damping parameters are 'c = 7.8 N·s/m' for the case of high damping and 'c = 3.5 N·s/m' for the case of low damping. By considering the numerical errors on the estimation of the ILEs, the results show good agreement with the results of the force-state mapping method.

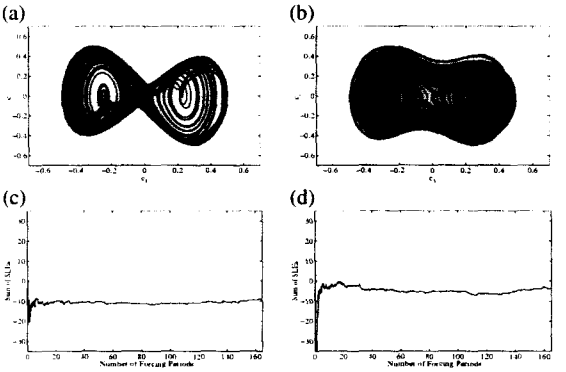

Fig. 12 (a) Pseudo phase portrait by the SVD (high damping)
(b) Pseudo phase portrait by the SVD (low damping)
(c) Sum of SLEs (high damping)
(d) Sum of SLEs (low damping)

Now, consider that the damping of the system is changed at a certain time (at 130 forcing period in this case). The sum of Lyapunov exponents and the sum of SLEs are shown in Fig. 13(a) and (b) respectively. From the sum of Lyapunov exponents, it is almost impossible to notice the change. However, we can see the distinctive change especially after about 160 forcing periods from the sum of SLEs as shown in Fig. 13(b).

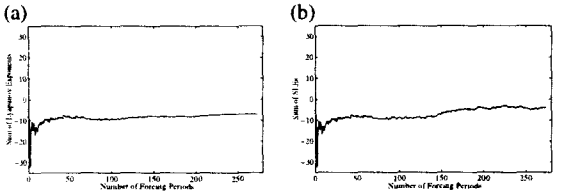

Fig. 13 Damping of the system is changed at about 130 forcing periods
(a) Sum of Lyapunov exponents (the change is not clear)
(b) Sum of SLEs (the change is clear)

Conclusion

In this paper, the force-state mapping method and the sum of SLEs have been successfully applied to a practical experimental set-up. To the authors' knowledge, it is the first time that the force-state mapping method has been successfully applied to a chaotic system. For a chaotic system, the results of the force-state mapping method are compared with the results of the sum of SLEs. Both methods have their own advantages and disadvantages. The results of the force-state mapping method and the sum of SLEs are summarised in Table 1.

Table 1. Summary of the experimental results

Cases		c (N·s/m)	k (kN/m)	α (kN/m)	β (MN/m^3)
Force-state Mapping method	Linear (low damping)	2.7±0.8	1.0±0.1		
	Linear (high damping)	7.3±0.6	1.0±0.1		
	chaos (low damping)	3.0±1.2		1.4±0.2	54.9±0.6
	chaos (high damping)	8.6±1.2		1.3±0.1	56.1±0.6
Sum of SLEs	chaos (low damping)	3.5±1.1			
	chaos (high damping)	7.8±0.9			

These results are obtained using four segments of the experimental data. From this, it is shown that there is good agreement between the two methods, i.e., the damping parameter estimated by these two methods is very similar. As shown in Table 1, the force-state mapping method has the ability to obtain all the necessary system parameters while the sum of SLEs can estimate only the normalised damping of the system. However, the sum of SLEs has some other advantages. First, one can detect the changes of damping of the system. Second, there is no requirement for knowledge of all the state variables, mass and forcing signals. Thus, in conclusion, if we do not require the details of system parameters but want to track the damping property, the sum of SLEs may be successfully applied.

References

1. Moon, F. C., and Holmes, P. J., "A Magnetic Strange Attractor," Journal of Sound and Vibration, Vol. 65 No. 2, pp. 275-296, 1979.

2. Marsi, S. F., and Caughey, T. K., "A Nonparametric Identification Technique for Nonlinear Dynamic Problems," Transactions of the ASME: Journal of Applied Mechanics, Vol. 46, pp. 433-447, 1979.
3. O'Donnell, K. J., and Crawley, E. F., "Identification of Non-linear Parameters in Space Structure Joints Using Force-State Mapping Technique," Space Systems Laboratory, Massachusetts Institute of Technology, Cambridge, Rept. #16-85, 1985.
4. Crawley, E. F., and Aubert, A. C., "Identification of Nonlinear Structural Elements by Force-State Mapping," AIAA Journal Vol. 24 No. 1, pp. 155-162, 1986.
5. Crawley, E. F., and O'Donnell, K. J., "Identification of Nonlinear System Parameters in Joints Using the Force-State Mapping Technique," Collection of Technical Papers - AIAA/ASME/ASCE/AHS Structures, Structural Dynamics & Materials Conference 27th, Vol. 1, pp. 659-667, 1986.
6. Crawley, E. F., and O'Donnell K. J., "Incorporation of the Effects of Material Damping and Nonlinearities on the Dynamics of Space Structures," Proceedings of the U.S. National Congress of Applied Mechanics 10th, pp. 415-420, pp 415-420, 1986.
7. Crawley, E. F., and O'Donnell, K. J., "Force-State Mapping Identification of Nonlinear Joints," AIAA Journal, Vol. 25 No. 7, pp. 1003-1010, 1987.
8. Worden, K., and Tomlinson, G. R., "Developments in Force State Mapping for Nonlinear Systems," Proceedings of the 6th International Modal Analysis Conference, Vol. 2, pp. 1471-1479, 1988.
9. Worden, K., and Tomlinson, G. R., "Application of the Restoring Force Surface Method to Nonlinear Elements," Proceedings of the 7th International Modal Analysis Conference, Vol. 2, pp. 1347-1355, 1989.
10. Surace, C., Worden, K., and Tomlinson G. R., "On the Non-linear Characteristics of Automotive Shock Absorbers," Technical Paper, Proceedings of the Institution of Mechanical Engineers. Part D, Journal of Automobile Engineering, Vol. 206, 1992.
11. Al-Hadid, M. A., and Wright, J. R., "Developments in the Force-State Mapping Technique for Non-linear Systems and the Extension to the Location of Non-Linear Elements in a Lumped-Parameter System," Mechanical Systems and Signal Processing, Vol. 3 No. 3, pp. 269-290, 1989.
12. Al-Hadid, M. A., and Wright, J. R., "Application of the Force-State Mapping Approach to the Identification of Non-linear Systems," Mechanical Systems and Signal Processing, Vol. 4 No. 6, pp. 463-482, 1990.
13. Wright, J. R., and Al-Hadid, M. A., "Sensitivity of the Force-State Mapping Approach to Measurement Errors," The International Journal of Analytical and Experimental Modal Analysis, Vol. 6 No. 2, pp. 89-103, 1991.
14. Al-Hadid, M. A., and Wright, J. R., "A Method for the Estimation of Mass and Modal Mass in the Identification of Nonlinear Single and Multi Degree of Freedom Systems Using the Force-State Mapping Approach," Structural Dynamics: Recent Advances, Proceedings of the 5th International Conference, pp. 399-410, 1991.
15. Al-Hadid, M. A., and Wright, J. R., "Estimation of Mass and Modal Mass in the Identification of Nonlinear Single and Multi Degree of Freedom Systems Using the Force-State Mapping Approach," Mechanical Systems and Signal Processing, Vol. 6 No. 4, pp. 381-401, 1992.
16. Lo, H. R., "System Characterisation and Identification of Non-Linear Systems (With Particular Reference to Hysteretic Systems)," PhD Thesis., Institute of Sound and Vibration Research, University of Southampton, 1988
17. Penny, J., and Linfield, G., "Numerical Methods using Matlab", Ellis Horwood, 1995.
18. Shin K., "Characterisation and Identification of Chaotic Dynamical Systems," PhD Thesis, Institute of Sound and Vibration Research, University of Southampton, 1996.